Separation and Purification Technology 251 (2020) 117406

Contents lists available at ScienceDirect

Separation and Purification Technology

journal homepage: www.elsevier.com/locate/seppur

Membrane-supported metal organic framework based nanopacked bed for protection against toxic vapors and gases

Yufeng Song[a], John Chau[a], Kamalesh K. Sirkar[a,*], Gregory W. Peterson[b], Uwe Beuscher[c]

[a] Otto York Department of Chemical and Materials Engineering, New Jersey Institute of Technology, University Heights, Newark, NJ 07102, United States
[b] US Army Combat Capabilities Development Command Chemical Biological Center, FCDD-CBR-PF, Aberdeen Proving Ground, MD 21010-5424, United States
[c] W. L. Gore & Associates, Inc., Mercury Control Systems, Elkton, MD 21921, United States

ARTICLE INFO

Keywords:
MOF-filled ePTFE membrane
High moisture permeability
Barrier to ammonia and chlorine
Defend against CEES

ABSTRACT

Defense against small molecule toxic gases is an important aspect of protection against chemical and biological threat as well as chemical releases from industrial accidents. Current protective respirators/garments cannot effectively block small molecule toxic gases and vapors and retain moisture transmission capability without a heavy burden. Here, we developed a nanopacked bed of nanoparticles of UiO-66-NH_2 metal organic framework (MOF) by synthesizing them in the pores of microporous expanded polytetrafluoroethylene (ePTFE) membranes. The submicron scale size of membrane pores ensures a large surface area of MOF nanoparticles which can capture/adsorb and react with toxic gas molecules efficiently. It was demonstrated that the microporous ePTFE membrane with UiO-66-NH_2 MOF grown inside and around the membrane can defend against ammonia for a significant length of time while allowing passage of moisture and nitrogen. It was also demonstrated that the MOF-loaded ePTFE membrane could provide significant protection from Cl_2 intrusion as well as intrusion from 2-chloroethyl ethyl sulfide (CEES) (a simulant for sulfur mustard). Such MOF-filled membranes exhausted by NH_3 breakthrough experiments were regenerated conveniently by heating at 60 °C for one week under vacuum for further/repeated use; a single regenerated membrane could block NH_3 for 200–300 min. The moisture permeability of such a membrane/nanopacked bed was considerably above the breathability threshold value of 2000 g/m^2 -day. The results suggest that microporous membranes filled with reactive MOF nanoparticles could be designed as protective barriers against toxic gases/vapors, e.g., NH_3 and Cl_2 and yet be substantially permeable to H_2O and air.

1. Introduction

Extensive research has been undertaken to develop novel materials, material structures and methods for improved protection against exposures to chemical and biological threat (CBT). The ultimate goal is to develop protective garments against such exposures. An account of earlier research and approaches is available [1]. The basic challenge in terms of light and thin protective clothing is to completely block transmission of chemical warfare (CW) agents [2] but achieve an optimal balance of the H_2O permeability and high chemical resistance [3]. The thermal burden should also be minimal [4–6]. This capability must exist for extended periods of time to allow extended/long missions in hazardous environments. Gloves/masks etc. made of butyl rubber are almost total blockage barriers but lack moisture transmission capability.

A subclass of personal protective equipment (PPE) involves protection against toxic gases and vapors released during industrial accidents. Current protective respirators/garments employ an extensive amount of porous sorbents e.g., active carbons (which can be impregnated with metal-salts for gas–solid reactions). As a result, these garments are very bulky. Such garments/respirators should be usable against a variety of toxic gases since the exact exposures are often unknown in sites of accidents; the gases and vapors include ammonia, chlorine, sulfur dioxide, hydrogen sulfide, hydrogen cyanide, cyanogen chloride etc. [7].

There have been a number of approaches to develop barriers to protect against various types of threats. Flexible membranes with aligned, sub-5 nm carbon nanotube (CNT) channels have been developed; they function as moisture conductive pores that can block virus etc. as a first step toward small molecular weight agent-responsive

Abbreviations: MOF, metal organic framework; CEES, 2-chloroethyl ethyl sulfide; ePTFE, expanded polytetrafluoroethylene; ECTFE, ethylene chlorotrifluoroethylene; H_2BDC-NH_2, 2-aminoterephthalic acid

* Corresponding author.
E-mail address: sirkar@njit.edu (K.K. Sirkar).

https://doi.org/10.1016/j.seppur.2020.117406
Received 29 February 2020; Received in revised form 14 July 2020; Accepted 15 July 2020
Available online 18 July 2020
1383-5866/

Nomenclature

A	open membrane area [cm^2]
$\Delta\bar{C}$	log mean concentration difference [kg/m^3]
ΔC_a	water vapor density difference between the two gas streams at left end of the flow cell [g/m^3]
ΔC_b	water vapor density difference between the two gas streams at right end of the flow cell [g/m^3]
C_{sat}	saturated water vapor density [g/m^3]
D_o	diffusion coefficient [cm^2/s]
D	effective diffusion coefficient [cm^2/s]
l	membrane thickness [μm]
L/D	the ratio of the thickness of membrane and the diameter of membrane pores
$\dot{m}/A$	mass flux of water vapor diffusing through the test sample [$kg/(m^2 \bullet s)$]
n	layers of ePTFE membranes
P_{sat}	the saturation water vapor pressure [Pa]
Q	volumetric flow rate [cm^3/min]
RH	relative humidity [%]
R_{tot}	total resistance to water vapor diffusion [s/m]
R_{BL}	resistance of boundary layers to water vapor diffusion [s/m]
R_{ePTFE}	resistance of one layer of ePTFE membrane to water vapor diffusion [s/m]
$R_{membrane}$	resistance of sample membranes to water vapor diffusion [s/m]
$R_{MOF\text{-}filled}$	resistance of one layer of MOF-filled ePTFE membrane to water vapor diffusion [s/m]
t_{lag}	time lag [min]
MVTR	moisture vapor transport rate [g/m^2·day]

protective barrier [8–9]. Metal-organic framework (MOF) UiO-66-NH_2 in the form of 20 × 40 mesh size granules in a packed bed showed significant sorption against ammonia and cyanogen chloride in breakthrough studies simulating protection filters and respirator cartridges [10]. Various functionalized variants of UiO-66 showed considerable capacity for ammonia removal via breakthrough measurements using dry and humid (80%RH) air [11]. The surface of the pores in covalent organic networks was chemically modified for better ammonia capture [12–13] for storage applications.

To use such gas/vapor capture/destruction properties of MOFs, an appropriate polymeric carrier/medium/filter would be useful in a protective garment. Mixed matrix membranes that are dense and have dispersed or layers of MOFs have been developed for various applications. These applications include organic solvent nanofiltration [14], water desalination [15], olefin-paraffin separation [16] etc. It is not known how such membranes will function as barriers for toxic gases. Those which involve MOFs distributed in a polymeric matrix will have to contend with interfacial compatibility; otherwise those interfacial regions become channels for leakage. The polymeric matrix may itself allow leakage. There are now thin membranes of MOF-5, for example [17]. It is not known what their barrier properties are vis-à-vis toxic gases. There are additional reports of the performance of MOF membranes [18,19]. Unless we have a membrane providing total blockage to start with, what is important to recognize is that a certain depth of sorbents is required to achieve protection via delayed breakthrough if in fact there are leakages. This is true for membranes in general even if we have extremely high selectivity of ~18000 as was achieved in CO_2-N_2 system [20].

To that end, what we have explored here involves synthesizing the MOF, UiO-66-NH_2, in the pores of thin microporous flat polymeric membranes; some synthesis takes place also on the surfaces of these membranes. The surface area that can be generated with nanocrystals located inside submicrometer membrane pores can be quite high. We can create a nanopacked bed in the porous structure of the membrane. The length to diameter ratios of pores in microporous membranes can be high facilitating the realization of many layers of MOFs. For example, the L/D ratio of a 0.45 μm pore size ePTFE membrane of thickness: 98 μm will be 217; the L/D ratio will be much larger if we employ nanoparticle diameter. As the gases migrate through the membrane pores, toxic species will diffuse and get adsorbed in and react with the MOF crystals. We have explored the NH_3 blocking capability of such membranes singly or stacked together in terms of determining the breakthrough time. For simplicity, this has been studied in flow-through mode using (1) an ammonia analyzer with ammonia measuring chips as well as (2) a gas chromatograph although the application for protective garments, of course, is a crossflow or diffusion mode.

Successful hydrothermal synthesis of the MOF, UiO-66-NH_2, is usually carried out in high boiling polar aprotic solvents e.g., DMF. It has been synthesized also using equimolar amounts of $ZrCl_4$ and $H_2BDC\text{-}NH_2$ in acetone [21–23]. Such solvents attack/swell most polymeric membranes. On the other hand, ePTFE-based membranes are unaffected by such solvents; however, porous ePTFE membrane is not wetted by polar aprotic solvents such as, DMF. We solved this problem by employing mixed solvents and carried out MOF synthesis within and outside microporous ePTFE membranes.

Using such MOF crystal-filled membrane pores and membrane surfaces as flat films, single or stacked, we explored their capacity to block breakthrough of NH_3 present in N_2 as carrier gas with or without humidity using ammonia chips. In addition, we investigated the individual breakthrough behavior of NH_3 and Cl_2 through such membrane-supported nanopacked beds in flow-through mode using a gas chromatograph. For testing the breakthrough of 2-chloroethyl ethyl sulfide (CEES) (a simulant for sulfur mustard) a permeation mode-based method using cross-flow was used [24,25]. We have also measured moisture permeability of such structures to evaluate their potential utility in protecting personnel from emissions at locations of industrial accidents. This involved a cross-flow configuration. Repeated use of such a structure to block gases/vapors was investigated by regenerating the MOF-loaded membranes which had experienced ammonia breakthrough and then restudying their ammonia breakthrough behavior.

2. Materials and methods

2.1. Materials and Chemicals

Hydrophobic expanded polytetrafluoroethylene (ePTFE) membranes (M − 045, pore size: 0.45 μm, porosity: 80%, thickness: 98 μm; GMM-404: pore size, 0.45 μm; porosity, 80%; thickness, 79 μm; W.L. Gore, Elkton, MD) were used in this study. Hydrophobic ethylene chlorotrifluoroethylene (ECTFE) membrane (3M, St. Paul, MN) (nominal pore size, 0.2 μm; thickness, 0.05 mm; porosity, 0.65) was used in ammonia breakthrough tests as the top sieving screen. Methanol (EMD Millipore, ≥ 99.8%), DMF (Fisher Chemical, 99.9%), zirconium (IV) chloride (Alfa Aesar™, > 99.5%), 2-aminoterephthalic acid ($H_2BDC\text{-}NH_2$, Acros Organics™, 99%) were used for UiO-66-NH_2 MOF synthesis. UiO-66-NH_2 MOF sample (TDA Inc., Wheat Ridge, Colorado; identified as TDA MOF).

2.2. MOF synthesis

UiO-66-NH_2 was synthesized using equimolar amounts of $ZrCl_4$ and $H_2BDC\text{-}NH_2$ in various proportions of DMF-methanol (pure DMF; 80% DMF-20% methanol; 50% DMF-50% methanol; 10% DMF-90%

methanol) in a Teflon-lined sealed vessel at 120 °C for 18 hr. After cooling to room temperature, the crystals were taken out and washed using DMF and methanol. Then, crystals were dried at 80 °C over 96 hr under vacuum.

2.3. MOF synthesis in ePTFE membrane

The following method was developed for synthesizing UiO-66-NH_2 MOF in the submicrometer pores and around hydrophobic ePTFE membrane. First, an ePTFE membrane was treated such that it had 80% (w/w) DMF and 20% (w/w) methanol in the pores. This was done by adding pure methanol into a sealed vessel with pieces of ePTFE membranes (methanol wets the pores right away), then adding DMF to increase the percent of DMF in the mixed solvent by 10% on a daily basis. Ultimately, the ePTFE membrane which was wetted by 80% (w/w) DMF and 20% methanol was immersed in a solution having a high concentration of reactants in the solution (10 mmol H_2BDC-NH_2 and 10 mmol $ZrCl_4$ dissolved in 25 g DMF-methanol mixture (80% DMF, w/w)). The membrane underwent shaking during the soaking process in a digital orbital shaker (Model SK-O180-Pro, SCILOGEX).

The sealed Teflon-lined pressure vessel was put next into an oven at 120 °C for 18 hr. The membrane was washed with DMF and methanol after the treatment. The membrane was next dried at 50 °C for 4 days under vacuum. This whole process was repeated 2, 3 or 4 times to achieve higher membrane weight gain resulting from UiO-66-NH_2 growth over existing growth. Experiments were also done with previously dried samples (50 °C for 4 days under vacuum and kept in a closed bottle with dessicants) as follows: 80 °C degassing for 5 hrs. followed by 160 °C degassing for 6 hr.

Henceforth GMM-404-104% means a degassed GMM-404 membrane with 104% weight gain.

2.4. Characterization of MOF and MOF-filled membrane

Empyrean multipurpose powder X-ray diffractometer with PIXcel^{1D} detector (Serial 202627, PANalytical) was used to obtain the powder X-Ray diffraction patterns (PXRD) of H_2BDC-NH_2, $ZrCl_4$, and UiO-66-NH_2. PXRD patterns of all samples were scanned by Cu K(alpha) radiation (λ = 1.54 Å, 40 mA, 45 kV) from 2° to 60° of 2θ, step size = 0.0260° (2θ), scan step time = 99.176 s. Fourier-transform infrared spectroscopy (FTIR) was carried out in an Agilent Cary 670 FTIR spectrometer for FTIR spectra of samples. 32 scans were taken for each sample over 6000–400 cm^{-1} with a resolution of 4 cm^{-1}.

Scanning electron microscopy (SEM) was implemented using two separate field emission-scanning electron microscopes (FE-SEM, Model LEO1530vp and JSM-7900F) to obtain the membrane cross sectional images. The samples were mounted on the SEM stubs by carbon tape and coated with 8 nm of gold by Turbomolecular pumped coater (Model EMS Q150T ES).

N_2 isotherm curves of samples were collected by an automated gas sorption analyzer (Model #: ASIQM000000-6, Quantachrome Instruments, Boynton Beach, FL). Pore size distribution and *Brunauer-Emmett-Teller* (BET) surface area were calculated by commercial DFT software combined with the instrument operation interface. Before starting BET measurement, membrane samples were degassed at 70 °C for 48 hr and UiO-66-NH_2 MOF samples were degassed at 120 °C for 18 hr .

2.5. Ammonia breakthrough experiment

Ammonia calibration gas was used as one of the toxic gases to test the efficiency of the final sorptive/reactive barrier product. The ammonia breakthrough testing was done using two different flow-through set ups. The dead-end set up for most of the testing using NH_3-sensing chips by the flow-through mode is shown in Fig. S1.

A stream of 100 ppmv ammonia in N_2 calibration gas (Gasco, Oldsmar, FL) was mixed with dry or wet N_2 gas before introducing mixed gases into the test cell. The flow rates of these two streams were adjusted by mass flow rate controllers (Model 8272-0453 and 829-C4212T, Matheson–Trigas, Montgomeryville, PA). The cell outlet NH_3 concentration was determined by a CMS analyzer (Draeger, Telford, PA) with ammonia CMS chips (10 – 150 ppmv, Model 6406020, Draeger, Telford, PA); sometimes an ammonia analyzer with a low detection range (1–100 ppmv, Model AR8500, Smart Sensor, Dongguan, China) was used for exploratory purposes. The membrane sample to be tested was put inside the cell. A piece of ECTFE membrane was put on top of the membrane to be tested to improve flow distribution over the membrane cross-section. Additional experiments were done with a virgin ePTFE membrane; these membranes were used as substrates for MOF synthesis. The open area of the membrane in the cell was 1.9 cm in diameter.

Two other dead-end breakthrough setups using ammonia chips were developed based on what is shown in Fig. S1. In one of the arrangements, there was no humidification of the N_2 gas, so that measurements could be made in the absence of moisture. In another setup, there was no UHP N_2 cylinder to eliminate dilution of the NH_3 concentration in the feed gas; the 100 ppmv NH_3-containing N_2 gas was fed directly into the test cell. The gas flow rates used were varied so that the same rate of NH_3 introduction may be maintained if needed. Another dead-end testing method, a microbreakthrough method, has been described in reference [11]. It was used here for NH_3 as well; it is described below in Section 2.7 in terms of microbreakthrough testing of Cl_2 in air.

2.6. Regeneration of membrane spent with NH_3

Pieces of GMM-404–144% MOF membranes used in the ammonia breakthrough testing described above with 50 ppmv dry or wet ammonia calibration gases were regenerated by heating at 60 °C for one week under vacuum. Then, the performances of regenerated MOF-filled membranes were tested using steps of Section 2.5.

2.7. Chlorine and CEES breakthrough experiments

Chlorine microbreakthrough testing using a set-up described in [11] was conducted on the material to determine the available capacity of the MOF embedded within the membrane. ~0.03 g of the composite was loaded into a 4 mm i.d. fritted glass tube and activated at 120 °C for 1 hr. Once activated, the tube was submerged in a water bath operating at 20 °C. A stainless steel ballast was charged with a predetermined quantity of chlorine, delivered via mass flow controller to a dry diluent air stream at a rate necessary to achieve 2000 mg/m^3, and then fed to the fritted glass tube. The effluent was monitored continuously using a HP6890 gas chromatograph equipped with a photoionization detector and an 11.7 eV lamp. The effluent breakthrough curve was integrated and subtracted from the total chlorine delivered to calculate the capacity of the composite.

The permeation of CEES was studied using the ASTM method F739-12 described in [24,25]. This was a sweep gas-based permeation method as opposed to a dead-end method.

2.8. Moisture vapor permeability measurement

A cross-flow method-based apparatus for moisture permeability measurement shown in Fig. S2 was developed based on [26]. The open membrane area was rectangular, 2 cm × 5 cm. Dry ultra-high purity N_2 (UHP NI 300, Airgas, Oakland, NJ) was passed through mass flow controllers (Model 8272-0417, Matheson–Trigas, Montgomeryville, PA). These two mass flow controllers were connected to a multiple flow controller (Model 8274, Montgomeryville, PA) via Ethernet cables to control the feed flow rates. A differential pressure transducer (Model 220DD00001B2B, MKS Instruments, Duncanville, PA) was used to monitor the pressure difference between the two sides of the sample

membrane. This pressure difference was maintained at a very low level (< 5 mTorr). The upper N_2 gas stream was humidified. Relative humidities (RHs) of both streams were measured by two RH transducers (HMP76, Vaisala, Woburn, MA) before entering the cell with a membrane. Relative humidities of the exit streams were also determined with two other RH transducers (HMP76, Vaisala, Woburn, MA).

3. Results and discussion

3.1. UiO-66-NH_2 MOF synthesis with and without ePTFE membranes

Fig. 1 provides the PXRD patterns of the MOFs synthesized in three different solvent mixtures of DMF and methanol along with those of MOF from another source (TDA MOF characterized in [27]); the PXRD patterns of the chemicals, $ZrCl_4$ and $H_2BDC\text{-}NH_2$, used to synthesize the MOF are also included. These results demonstrate that the PXRD patterns of UiO-66-NH_2 MOFs synthesized in this study are identical to the known PXRD patterns for this MOF; two highest diffraction peaks at $2\theta = 7.3^\circ$ and 8.5° correspond to its d-spacing of 12.1 Å and 10.5 Å. Fig. 1 also shows the PXRD patterns of the virgin ePTFE GMM-404 membrane and this ePTFE membrane with MOF synthesized inside.

FTIR spectra (references [28,29] are useful in this regard) of a variety of samples are shown in Fig. 2. These include the data obtained from the UiO-66-NH_2 MOF synthesized with different proportions of DMF-methanol in the reaction chamber. Because of the acidic proton of a carboxylic acid is replaced by a different cation to form a carboxylate, the absorption band around 1673 cm^{-1} of the carboxylic acid group disappears, and two bands between 1566 cm^{-1} and 1400 cm^{-1} appear instead; the bands correspond to the antisymmetric and symmetrical stretching and bending vibration of the structure. The peaks at 659 cm^{-1} and 477 cm^{-1} are also associated with Zr–(OC) bond. These spectra demonstrate that this MOF could be successfully synthesized using equimolar amounts of $ZrCl_4$ and $H_2BDC\text{-}NH_2$ in various proportions of DMF-methanol in the membrane pores; spectra for M − 045 ePTFE membrane with and without exposure to ammonia are also included along with those of the two reactants used in synthesis and the TDA MOF.

The ePTFE porous membrane could be wetted by a low percent (10%, w/w) of DMF in methanol after several hours of soaking (See related discussion in SI after Fig. S2). The weight gain of membrane under these condition due to UiO-66-NH_2 MOF growth inside of membrane pores and on the surface of membrane was only ~2%. This

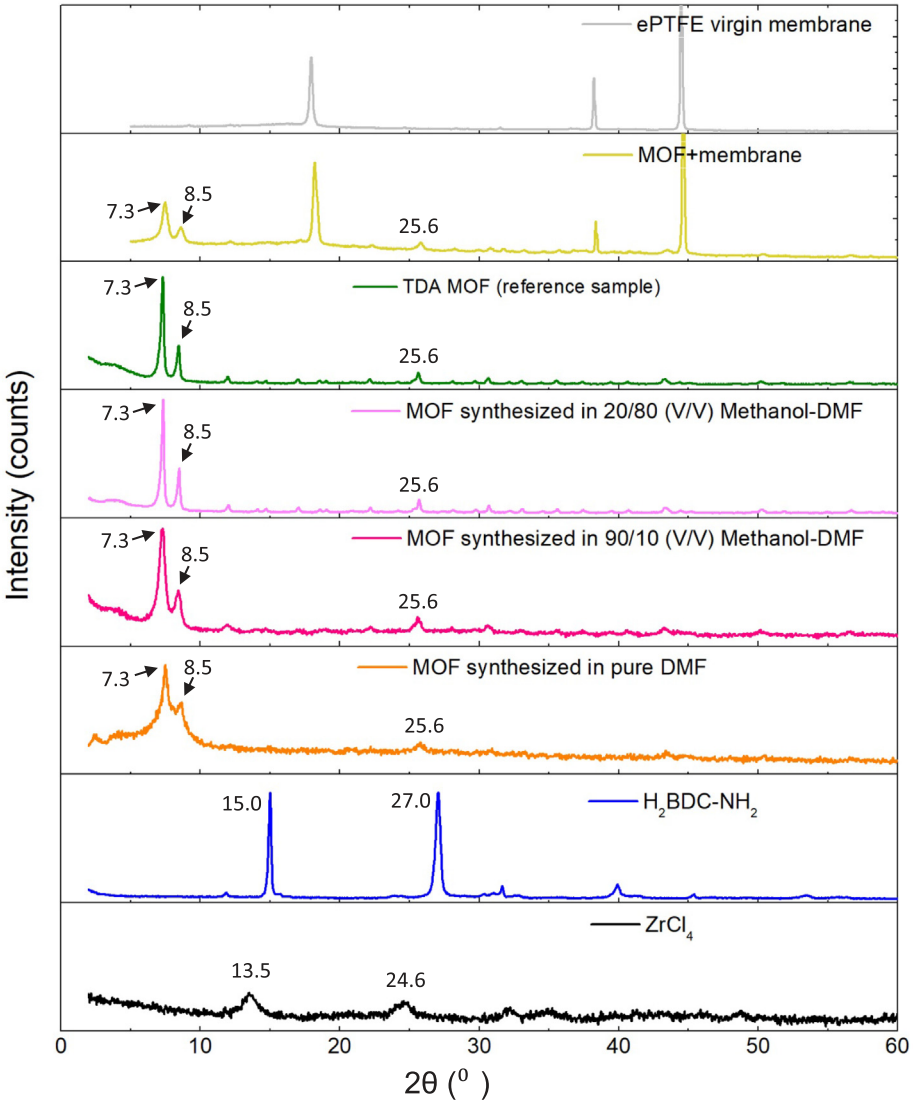

Fig. 1. PXRD patterns of 2θ from 2° to 60° of UiO-66-NH_2 synthesized in various proportion of DMF-methanol (pure DMF, 80% (w/w) DMF and 20% methanol, 10% (w/w) DMF and 90% methanol) and TDA MOF; PXRD patterns of $H_2BDC\text{-}NH_2$, $ZrCl_4$ are at the bottom; PXRD patterns of virgin ePTFE GMM-404 membrane and this ePTFE with MOF are at the top.

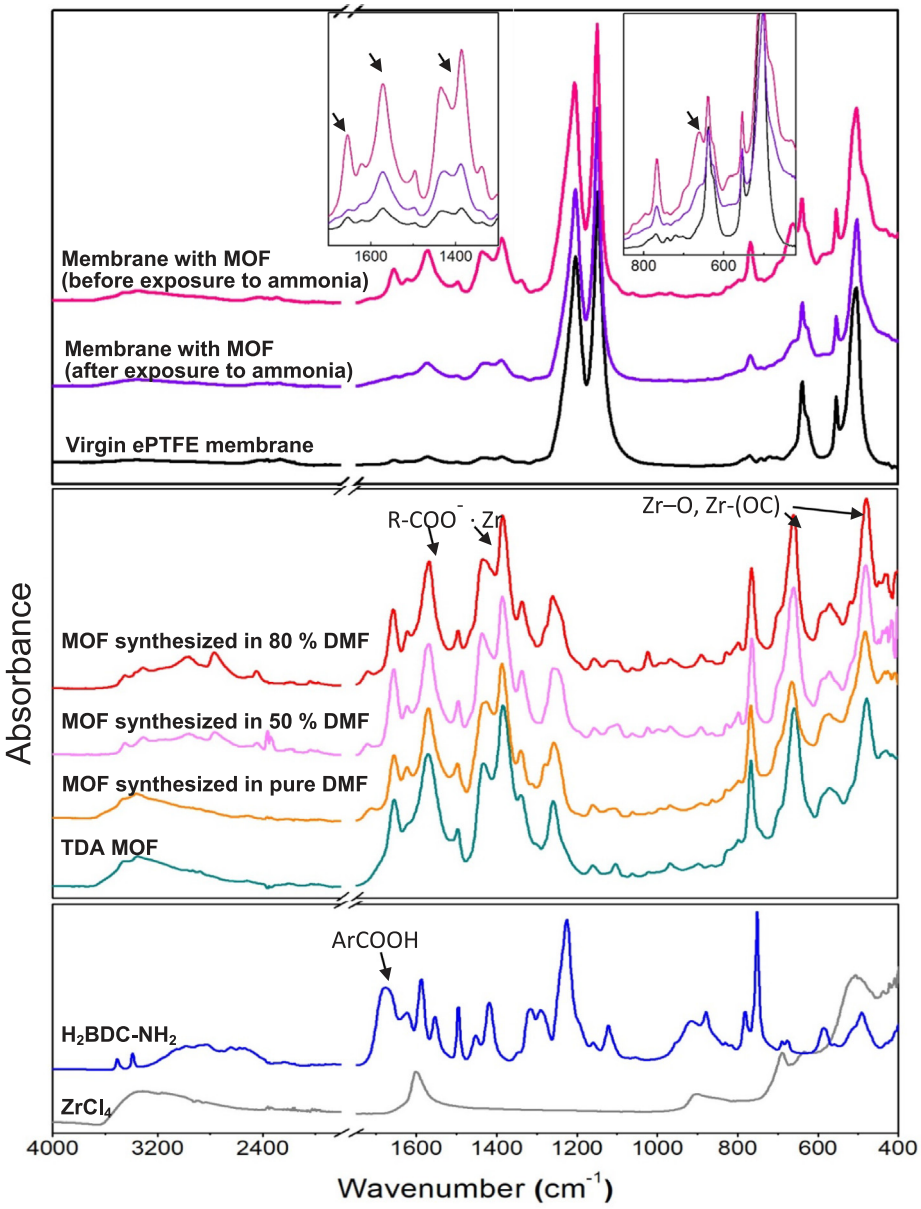

Fig. 2. The 4000 to 400 cm^{-1} range of FTIR absorption spectra of UiO-66-NH_2 synthesized in various proportions of DMF-methanol (pure DMF, 80% (w/w) DMF and 20% methanol, 50% (w/w) DMF and 50% methanol, 10% (w/w) DMF and 90% methanol), sample from another source (TDA MOF)), coarse crystal MOF, virgin ePTFE (M − 045) membrane, ePTFE (M − 045) with UiO-66-NH_2 MOF before and after exposure to ammonia; spectra for reactants $ZrCl_4$ and $H_2BDC\text{-}NH_2$ included.

was achieved during the trial of soaking ePTFE membrane in a solution obtained by mixing $H_2BDC\text{-}NH_2$ solution (2 mmol $H_2BDC\text{-}NH_2$ dissolved in 4.7 g DMF and 25 g methanol) and $ZrCl_4$ solution (2 mmol $ZrCl_4$ Dissolved in 15.3 g methanol). Extended soaking time and repeated reaction trials could increase the MOF weight gain. However, this process was not very efficient.

For obtaining high weight gain in each trial, the concentration of each reactant in the mixing solution was increased. DMF was needed for dissolving the $H_2BDC\text{-}NH_2$; methanol assisted in dissolving $ZrCl_4$. There is a solubility limitation of $H_2BDC\text{-}NH_2$ in DMF. For dissolving10 mmol $H_2BDC\text{-}NH_2$, 19 g is the least amount of DMF needed (at room temperature). Although adding

2.5 g (~10% w/w) methanol would let 10 mmol $ZrCl_4$ get dissolved, 5 g of methanol was added to avoid fluctuations introduced by methanol evaporation.

In order to achieve high concentrations of reactants in the solution, a mixture of 80% w/w DMF and 20% w/w methanol was used as the solvent. The weight gains of ePTFE membranes due to the growth of MOFs inside the pores and on the surface of the membrane under these conditions are shown in Fig. 3. Repeating this process, the values of % weight gain achieved by a synthesis process repeated 2 times, 3 times, 4 times are also shown in Fig. 3. This weight gain with respect to the bare membrane weight and the weight gain with respect to the total weight (= (virgin membrane weight + weight gain)) have different colors in this Figure. For example, 1 time % weight gain in Trial 1 for membrane M − 045 is 41% ((g/g) × 100). However, the weight % of MOF in the membrane is 29%, calculated from Eq. (1):

$$\text{Weight \% of MOF in the membrane} = \frac{\text{weight gain}}{\text{weight of virgin membrane} + \text{weight gain}} \times 100\% = \frac{0.41}{1+0.41} \times 100\% \approx 29\% \quad (1)$$

The weight gain of larger size membranes (Trials 2 and 3, dimension of larger size membrane: ~21 cm × 15 cm) is less than that in the smaller sizes (Trial 1, dimension of small size membrane: ~ 2.5 cm × 2

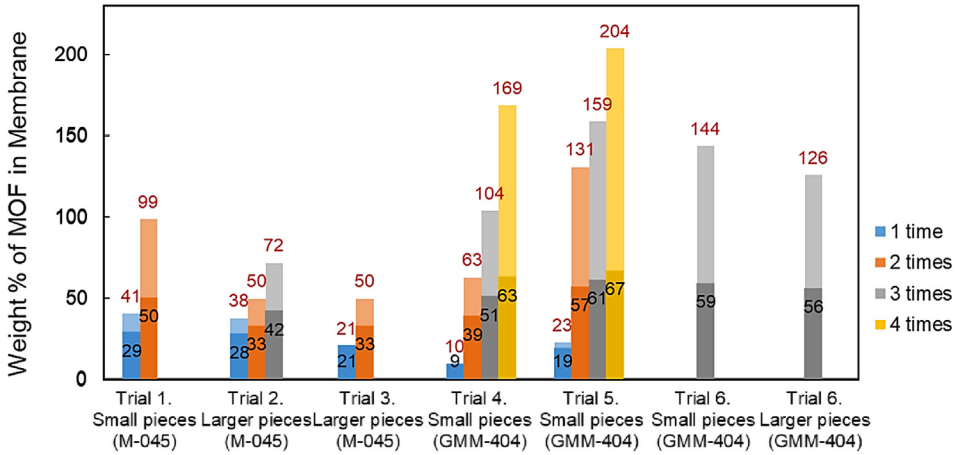

Fig. 3. Weight gain of ePTFE membranes due to the growth of MOFs. (The weight gain with respect to bare membrane weight is labeled in red; and the weight gain with respect to the total weight is labled in black.).

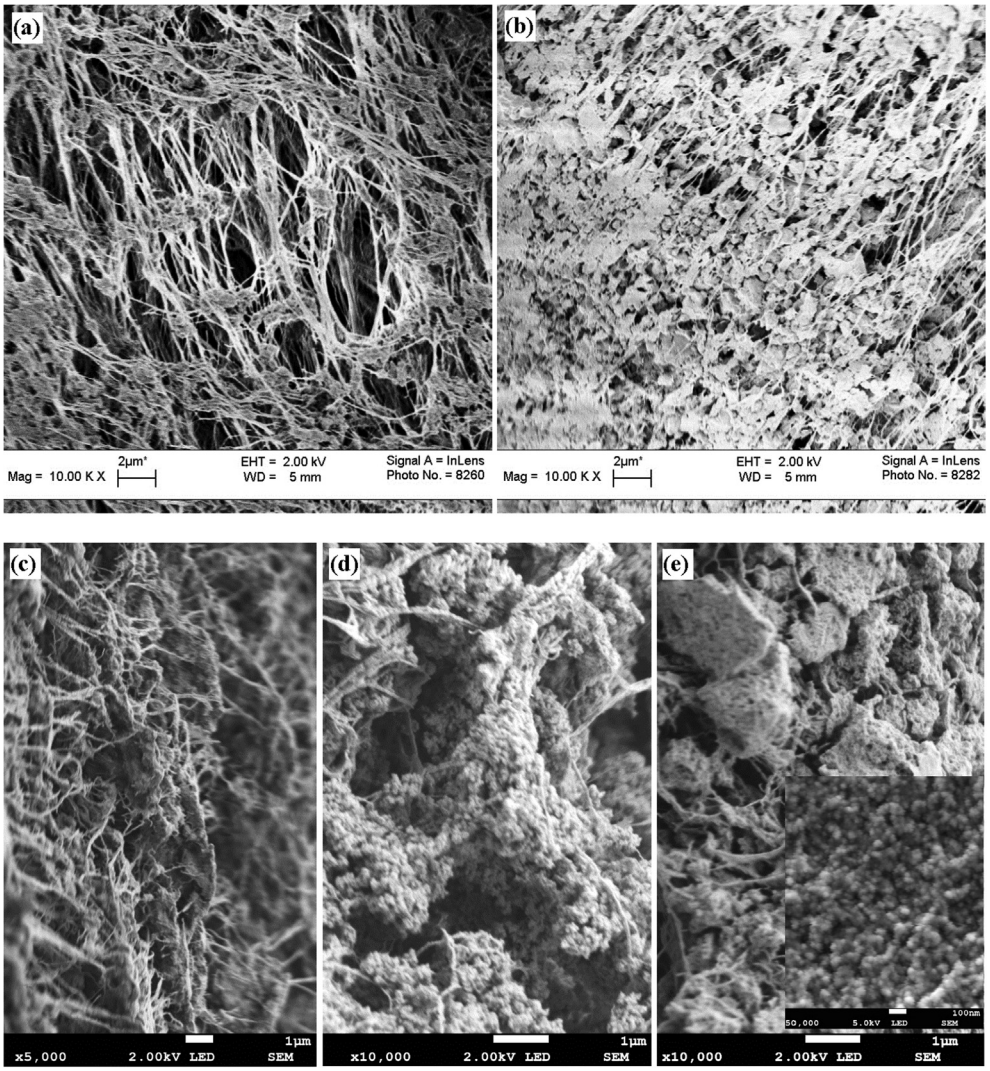

Fig. 4. SEM images of the cross section of (a) virgin ePTFE (M − 045) membrane; (b) M − 045 membrane with UiO-66-NH_2 MOF growth (3 times with total weight gain ~72%); (c) virgin ePTFE membrane (GMM-404); (d) GMM-404 membrane with UiO-66-NH_2 MOF growth (2 times with total weight gain ~63%); (e) GMM-404 membrane with UiO-66-NH_2 MOF growth (3 times with total weight gain ~144%); inset in (e) has a 100 nm scale; (a) and (b) were taken by LEO1530vp SEM; (c), (d) and (e) were taken by JSM-7900F SEM.

cm). This is due to the ePTFE membranes being folded 3–4 times to fit the vessel size. This leads not only to insufficient wetting of ePTFE membrane, but also to the loss of the MOFs attached on the membrane surface during washing and drying of the larger piece of membrane. The weight gain of larger pieces (Trial 6, dimension: ~ 2.5 cm × 5.0 cm) is a little less than those of smaller pieces (Trial 6, dimension: ~ 2.5 cm × 2.5 cm); this is also due to the membranes being slightly folded to fit the vessel size. The membranes used in Trials 4 and 5 were cut into round pieces of the same size (diameter: 4.7 cm). The weight gain of membranes in Trial 5 is higher than the weight gain in the trial 4, due to ePTFE membranes being soaked in the reactants solution for a longer period at room temperature. This allows achievement of a better exchange between the bulk solution and the solution inside of membrane pores, while the MOF crystal nuclei grow larger.

The SEM images of the cross section of the membranes shown in Fig. 4 demonstrate that MOF was successfully grown inside the pores of the ePTFE membranes (M−045 and GMM-404). Cross sectional images of M−045 membrane with UiO-66-NH_2 MOF growth (weight gain: ~72%) and GMM-404 membrane with UiO-66-NH_2 MOF growth (weight gain: ~63%) show that small MOF crumbs filled up most empty regions in the membrane pores. Besides, accumulation could be observed in the cross section of GMM-404 membrane with UiO-66-NH_2 MOF growth (wt. gain: ~144%). The MOF nanocrystals inside membrane pores appear to be tightly packed inside the fibrillar ePTFE membrane structure. Shaking the membrane does remove some particles from the membrane surface but do not dislodge those inside the pores as we have seen from repeated use. Fig. 4(e) has an inset with 100 nm scale; it shows a lot of crystals 100 nm or smaller. Per the PXRD in Fig. 1 we have crystals in the ePTFE membrane; hence we have nanocrystals. We do not expect any specific interaction between UiO-66-NH_2 MOF with a few hydrophilic functional groups and the pore surfaces of the highly hydrophobic PTFE membrane.

Fig. 5 plots N_2 adsorption and desorption isotherms for the following samples: virgin ePTFE membranes, ePTFE membranes with differing UiO-66-NH_2 MOF loadings, and TDA MOF; y-axis unit of cm^3/g refers to per gram of sample. The very sharp rise in the adsorbed volume in the plot at very low P/P_0 represents the narrow micropores (< ~ 1 nm). The approximately sharp turn and subsequent slow increase implies narrow mesopores (< ~ 2.5 nm) and macropores. The corresponding BET surface areas are listed in Table 1 (minus that for TDA MOF). The BET surface areas of MOF-filled ePTFE membranes have positive correlation with the percent loading of MOF in the ePTFE membranes. The surface area of MOF-filled ePTFE membranes with higher loading of MOF is closer to the surface area of fine powder grown without membrane. Pore size distributions were determined from N_2 isotherms by Density Functional Theory (DFT) characterization method and are shown in Fig. S3. The MOF UiO-66-NH_2 is related to UiO-66 and has a structure similar to UiO-66. Cavka et al. [21] estimate the window opening of UiO-66 to be ~ 6 Å. The small opening size however allows N_2 penetration into and out of the pores for adsorption/desorption. Fig. S3 shows that pore size distributions of various MOF samples of this work also have half window openings ~3–5 Å.

3.2. Breakthrough studies using MOF-filled membranes

Here we focus on testing the defense to a low concentration of ammonia in N_2 using first the set up shown in Fig. S1 and an ammonia analyzer using a chip. Draeger CMS analyzer tested with chips not only gave accurate reading at lower concentrations, but also was not affected by the long testing time. As shown in Fig. 6, a comparison of the breakthrough time for one layer of virgin ECTFE membrane (thickness: 50 μm, pore size 0.2 μm, porosity: 65%) without any MOFs (shown by curve h) with the breakthrough time of one layer of virgin ECTFE membranes (above) and one or three layers of ePTFE-MOF membranes (below) confirm that ePTFE membrane with UiO-66-NH_2 MOF growth effectively blocks ammonia gas for a significant period of time. Here breakthrough time indicates when ammonia appears first at the outlet of the cell and the NH_3 chip starts showing the first trace of blue color; that time was noted as the breakthrough time. The next point for each graph in the figure corresponds to an actual concentration value from the chip which was the lowest measurable value from the chip being used. No particular breakthrough concentration is therefore being specified in the region of breakthrough time. We were interested in complete blockage of NH_3 and we listed it as retention time (sometimes also as blocking time). There is an inset on the bottom right of Fig. 6 which provides an expanded view of this region for various systems.

Fig. 6 also shows the actual time when breakthrough happens is visible for each sample membrane. One layer of ePTFE (M−045) membrane with 63% weight gain due to MOF growth totally blocked ammonia present in feed gas (100 ppmv, flow rate 5 cm^3/min) for 31 min, which is the corrected total blocking time (31 min = 47 min for the composite (curve a) − 16 min for the single ECTFE membrane (curve h)), listed in Table S1. Correspondingly, one layer of ePTFE (GMM-404) membrane with 104% weight gain due to MOF growth shows a corrected total blocking time of 37 min for ammonia present in feed gas (100 ppmv, flow rate 5 cm^3/min). The total blockage time did not change much due to a change in the thickness of GMM-404 membrane (79 μm), which is 19 μm less than M−045 membrane; however the weight gain was somewhat higher. The intercepts of line b and line d with the time axis are close. Three layers of GMM-404 membrane with 204 wt% loading (curve c) displays a corrected total blocking time of 129 min for the dry 100 ppmv NH_3 containing gas. That these membranes are effective with wet feed gas is demonstrated by curves f and g. Comparison of the breakthrough times for dry gas with the breakthrough times for wet gas confirm that ePTFE membrane with

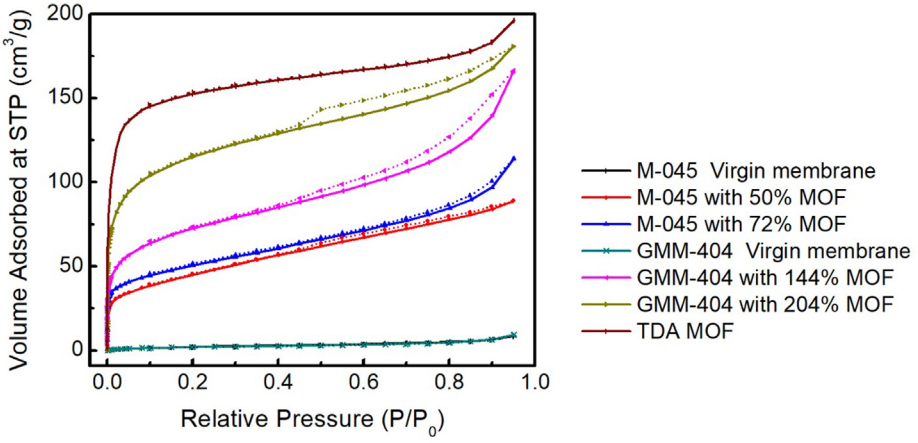

Fig. 5. N_2 isotherm plots at 77 K for UiO-66-NH_2 MOFs in virgin ePTFE membranes (M−045, GMM-404), ePTFE membrane with UiO-66-NH_2 MOF (M−045 with 50%, 72% MOF loading and GMM-404 with 144%, 204% MOF loading), and TDA MOF. Solid lines represent adsorption phase and dashed lines represent desorption phase.

Table 1
BET based surface area estimates.

Samples	Surface area (m^2/g)
Virgin ePTFE (M − 045) membrane	4.1
ePTFE (M − 045) membrane with UiO-66-NH_2 MOF growth (weight gain: ~ 50%).	132
ePTFE (M − 045) membrane with UiO-66-NH_2 MOF growth (weight gain: ~ 72%).	172
Virgin ePTFE (GMM-404) membrane	5.7
ePTFE (GMM-404) membrane with UiO-66-NH_2 MOF growth (weight gain: ~ 144%).	267
ePTFE (GMM-404) membrane with UiO-66-NH_2 MOF growth (weight gain: ~ 204%).	423
UiO-66-NH_2 MOF fine powder	513

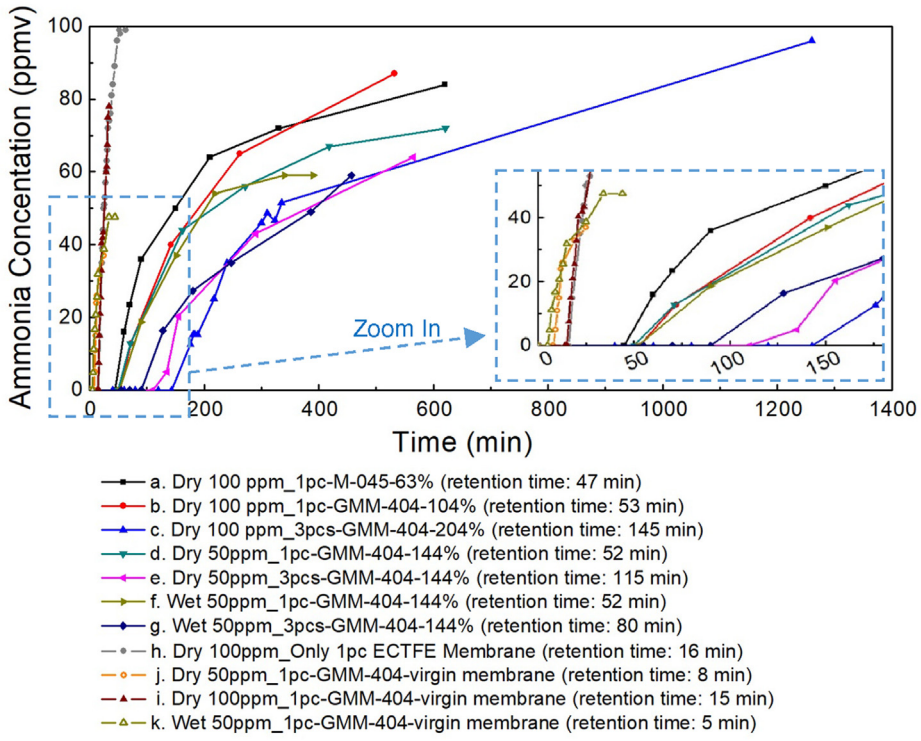

Fig. 6. Ammonia breakthrough tests with NH_3-containing gas stream having 100 ppmv (70.8 mg/m^3) flowing at 5 cm^3/min or 50 ppmv (35.4 mg/m^3) flowing at 10 cm^3/min through UiO-66-NH_2 MOF-loaded membranes; the top membrane is unfilled ECTFE. Results are provided also for ePTFE virgin membrane for various feed gas compositions; RH of dry stream was 0%; RH of wet stream was ~ 50%. Here 1 pc means one MOF-loaded membrane; 3 pcs mean three stacked MOF-loaded membranes.

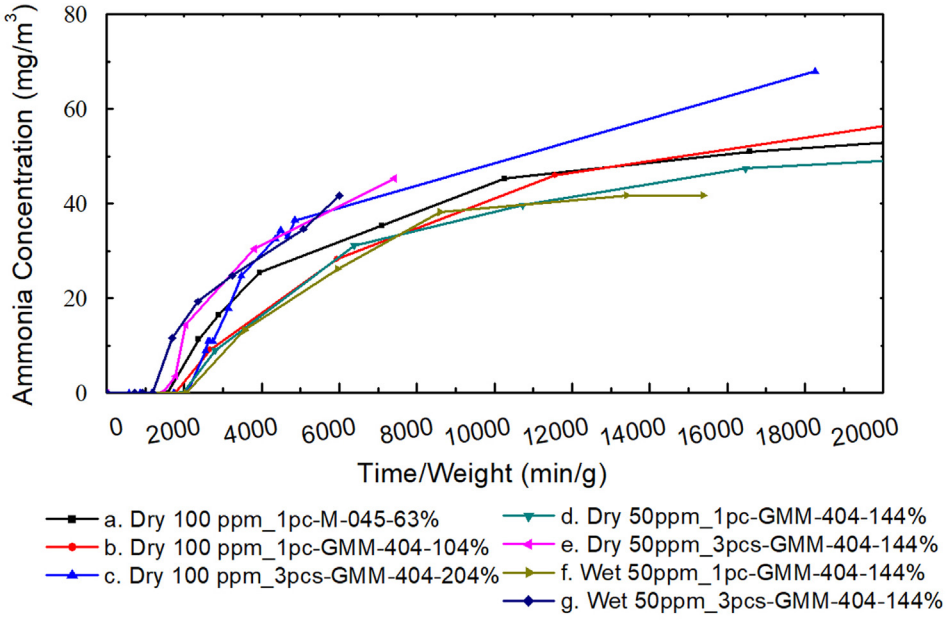

Fig. 7. Ammonia breakthrough test with 100 ppmv (70.8 mg/m^3) NH_3-containing gas stream having 100 ppmv (70.8 mg/m^3) flowing at 5 cm^3/min or 50 ppmv (35.4 mg/m^3) flowing at 10 cm^3/min through UiO-66-NH_2 MOF-loaded membranes normalized by membrane weight. The top membrane in each case is unfilled ECTFE. The contribution of void volume to time delay has been removed in this plot; (RH of dry stream was 0%; RH of wet stream was ~ 50%.).

UiO-66-NH_2 MOF growth effectively blocks ammonia gas under moist conditions as well (relative humidity (RH) ~50%).

Fig. 7 illustrates the ammonia breakthrough behavior normalized by the membrane weight; here the contribution of the void volume in connecting tubing etc. has been removed. Further, we have plotted the gas composition in units of mg/m^3; the conversion factor is given by Eq. (S.1). Here the contributions of cell chamber void volume and the void volume of tubing connected from testing cell to the analyzer were determined from the data in curves h-k of Fig. 6. The detectable reading of ammonia concentration delay for one piece of virgin ePTFE membrane with or without one layer of virgin ECTFE membrane was very close. The reading delay depended primarily on the volume of the system void. The delay was ~6 min for a flow rate of 10 cm^3/min; the delay was ~15 min for a flow rate at 5 cm^3/min.

Fig. 8 shows that the regenerated MOF-filled membranes retain the ability to defend ammonia present in the feed gas stream better than newly-made membranes. The performance of 59% MOF-filled GMM-404 membrane which was used after ammonia breakthrough testing with 50 ppmv dry ammonia calibration gas and then regenerated by heating at 60 °C for one week under vacuum is illustrated by curve ii. The breakthrough time is 310 min, a considerable improvement over freshly made samples. Curves v and vi show the performance of GMM-404-144% MOF membranes which were used after ammonia breakthrough testing with 50 ppmv wet ammonia calibration gas and then regenerated by heating at 60 °C one week under vacuum. The difference between curve ii and curve v (or vi) indicates that presence of moisture can impact the performance of regenerated MOF-filled membrane.

The ammonia breakthrough testing result of refreshed MOF-filled membrane is shown by curve i; this sample was stored in a container with dessicant for 1 year and then heated at 60 °C for one week under vacuum. The refreshed membrane has a significantly better performance than a newly-made membrane. One possible hypothesis is that it may be due to time-dependent restructuring of the MOFs in the submicron size pores reacting further at 60 °C. Curve iii shows the performance of an used MOF-filled membrane regenerated by passing pure nitrogen gas at 5 cm^3/min for 24 hr. The nitrogen gas stream removed only limited amounts of ammonia. Fig. S4 illustrates the breakthrough behavior of such regenerated membranes with time normalized with membrane weight (as in Fig. 8).

The results of microbreakthrough measurements of NH_3 using the gas chromatograph-based packed bed configuration of reference [11] are shown in Fig. 9(a) for the GMM membrane with 204% MOF loading. Ammonia capacity of this GMM membrane with 204% MOF loading was estimated to be 1.13 mol/kg. Typical values of MOF (from TDA Inc.) loading of NH_3 is 2.6 mol/kg for a packed bed of MOF pellets. Therefore the sorption capacity of the membrane-supported MOFs synthesized in submicrometer size membrane pores is considerable.

Chlorine breakthrough behavior was also studied (Fig. 9(a)) and the sorption capacity calculated to determine how accessible the MOF was within the membrane and its potential for use in a protective barrier or filter for a variety of toxic gases. Fig. S5 shows breakthrough as a function of time for the MOF-filled membrane for both gases with the gas composition in units of mg/m^3. It was determined from these data that chlorine loading capacity of the GMM membrane with 204% MOF loading was 1.679 mol/kg. The intrinsic loading capacity of the UiO-66-NH_2 MOF for Cl_2 is 5.21 mol/kg.

Fig. 9(b) shows the results of permeation studies in the cross-flow setup with CEES. The breakthrough happens around 46.4 min. This result allows one to develop an estimate of the effective diffusion coefficient for CEES through MOF-filled GMM-404 membrane (weight gain 204%, 67% MOF filled) using time lag information. Since time lag, t_{lag}, is related to the effective diffusion coefficient D_o and the membrane thickness by

$$t_{lag} = (l^2/6D_o) \quad (2)$$

where l is the membrane thickness (80 μm), one can calculate the effective diffusion coefficient of CEES in this membrane given t_{lag} to be 46.4 min, as shown in Fig. 9(b). This value is significantly larger than that through a graphene oxide (GO) based membrane [25]. On the other hand, the steady state permeation rate of CEES through the GO membrane is far smaller than what was observed here. The value of the effective diffusion coefficient, D_o, turns out to be 3.83 × 10^{-9} cm^2/s; this value is close to that through the rather impermeable butyl rubber (D_o = 2.64 × 10^{-9} cm^2/s) [30].

3.3. Moisture permeance measurement

Calculation of the mass transmission rate of water vapor per unit

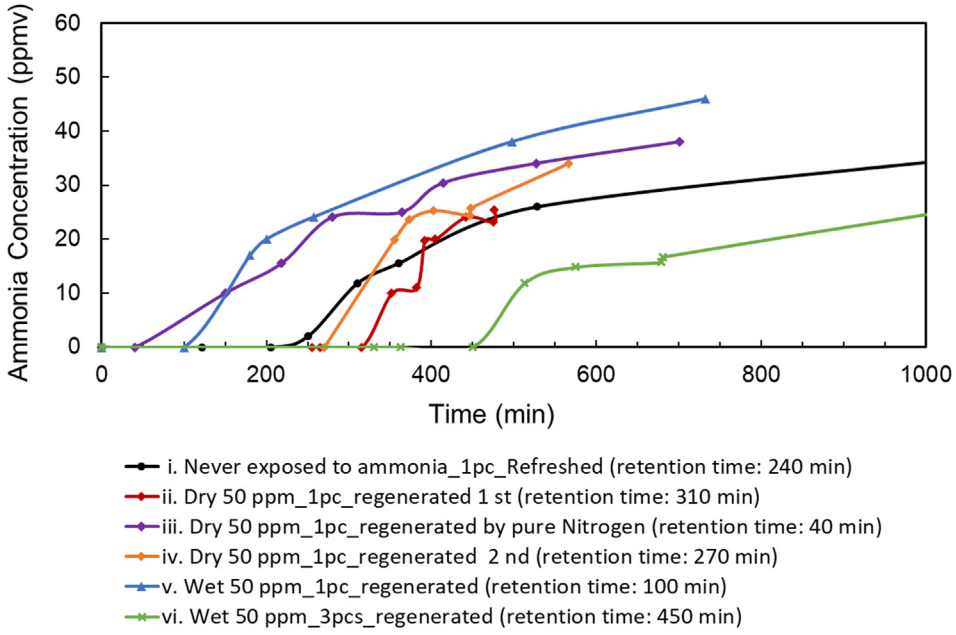

Fig. 8. Ammonia breakthrough test with dry or wet 50 ppmv (35.4 mg/m^3) NH_3-containing gas stream flowing at 10 cm^3/min through regenerated UiO-66-NH_2 MOF-loaded membranes; the top membrane is unfilled ECTFE (RH of dry stream was 0%).

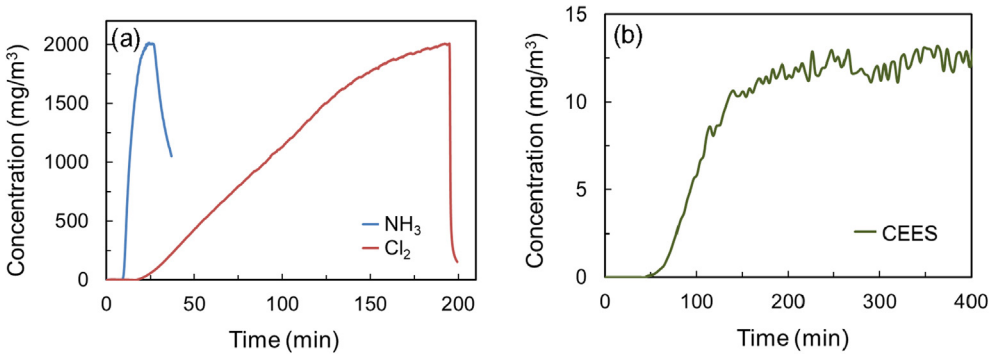

Fig. 9. (a) Ammonia breakthrough test in the microbreakthrough apparatus with composition monitoring by GC for GMM membrane with 204% MOF; chlorine breakthrough test for GMM-404 membrane with 204% UiO-66-NH_2 by 2000 mg/m^3 NH_3– or Cl_2-containing gas stream flowing at 20 cm^3/min. (b) CEES permeation test in cross-flow for GMM-404 membrane with 204% UiO-66-NH_2 MOF.

membrane area, $\dot{m}/A$, diffusing through the test membrane from one side of the membrane to the other was carried out using equations given near the end of the Supplementary information **(Appendix A)**. This employs a cross-flow configuration per Fig. S2 with essentially diffusion only mode since the pressure difference was extremely low (< 5 mTorr). The total resistance (R_{tot}) to water vapor diffusion through a sample was obtained from the linear relationship between logarithmic mean water vapor concentration difference ($\Delta\bar{C}$) (Eq. (3)) and the mass flux, ($\dot{m}/A$), which is also the moisture vapor transmission rate (denoted as MVTR) [26]. This relation is given by Equation (3):

$$\Delta\bar{C}\,(kg/m^3) = \frac{\Delta C_a - \Delta C_b}{\ln\left(\frac{\Delta C_a}{\Delta C_b}\right)} \tag{3}$$

$$\Delta\bar{C} = R_{tot} \times \left(\frac{\dot{m}}{A}\right) \tag{4}$$

where ΔC_a is the water vapor concentration difference between the two gas streams at one end of the flow cell and ΔC_b is the water vapor concentration difference between the two gas streams at the other end of the flow cell. Further,

$$R_{tot} = R_{BL} + R_{membrane} \tag{5}$$

which reflects the fact that there are two sources of transport resistance for moisture, the membrane resistance $R_{membrane}$ and the total boundary layer resistance R_{BL} on two sides of the membrane.

From the measured values of MVTR and ($\Delta\bar{C}$), one can calculate the values of R_{tot}. In Fig. S6, the vertical axis on the left hand side represents the values of R_{tot}. A plot of this value for various layers of empty ePTFE membranes (GMM-404) stacked one over the other is shown there. The intercept of this plot on the left hand vertical axis represents the total resistance of the boundary layers (R_{BL}) on the two sides of sample membrane sufaces; the slope indicates the intrinsic resistance of the empty sample membrane.

Fig. 10 illustrates the moisture vapor transmission rate (MVTR) as bars for a virgin ePTFE membrane and a MOF-filled ePTFE membrane (59% MOF GMM-404) based on the vertical axis on the left hand side [8]; the value of the total resistance to water vapor diffusion is shown on the right side vertical axis. Per Fig. S6, the value of R_{BL} is 217.7 s/m; it is drawn as a grey dashed horizontal line in Fig. 10. As shown in Fig. S6, the value of $R_{tot,\ ePTFE}$ is 228.3 s/m for one empty ePTFE membrane. So, for an empty ePTFE membrane, R_{ePTFE} is 11 s/m (=$R_{tot,\ ePTFE}$ - R_{BL} = 228.3 s/m – 217.7 s/m). From the data shown for a 59% MOF GMM-404 membrane in Fig. 10 by a blue dot, the $R_{MOF\text{-}filled}$ is 33 s/m. This result shows that the MVTR values are reduced very little from that for an empty membrane by the incorporation of MOF crystals in the submicrometer pores of the ePTFE membranes. Further the MVTR values remains much higher than the breathability limit of 2000 g/m^2–day [8]. Note that these measurements were done at 28 °C.

4. Concluding remarks

A method was developed to synthesize crystals of the MOF UiO-66-NH_2 in the submicrometer pores of an ePTFE microporous membrane and on its surfaces. Due to the submicrometer pore size of the membrane, the crystals inside the pores were nanocrystals generating a nanopacked bed with a very high L/D ratio. The method of growing nanocrystals inside the membrane pores involved developing a solvent exchange process at the beginning so that there is considerable amount of solvent DMF present inside the pores along with some methanol even though DMF does not wet ePTFE membranes. A solvent composition of 80% DMF and 20% methanol inside the membrane pores and outside (containing the reactants H_2BDC-NH_2 and $ZrCl_4$ in solution) was successfully used during MOF synthesis at 120 °C.

The resulting microporous reusable ePTFE membrane-based nanopacked bed of UiO-66-NH_2 MOFs in membrane pores and outside can defend against ammonia in N_2 for a significant length of time while allowing passage of moisture and nitrogen. A similar nanopacked bed of MOF-filled ePTFE membrane was able to block Cl_2 and CEES also for a considerable length of time. Although the overall sorption capacity of such nanopacked beds of MOF crystals in and around a microporous ePTFE membrane is lower than that of a packed bed of MOF microcrytsals, it is still considerable and is likely to be useful for development of a barrier against toxic gases and vapors. When such a membrane-supported nanopacked bed exhausted by ammonia breakthrough was regenerated by heating at 60 °C under vacuum for 7 days, ammonia blockage time for a single membrane was increased to 200–300 min. The water vapor transmission rate through such a barrier membrane was a few times higher than the breathability limit. A general technique has been developed for obtaining membrane-suported nanopacked beds of MOFs which may be successfully used as a protective barrier against toxic gases and vapors.

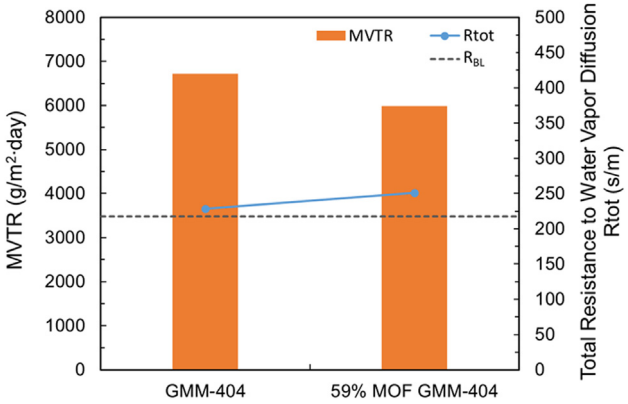

Fig. 10. MVTR (bar) and corresponding R_{tot} (line) of MOF-filled membranes and virgin ePTFE membranes (data collected at ~28 °C). 59% MOF GMM-404 is GMM-404 membrane with UiO-66-NH_2 MOF growth (weight gain: ~144%).

Declaration of Competing Interest

The authors declare that they have no known competing financial interests or personal relationships that could have appeared to influence the work reported in this paper.

Acknowledgement

The authors gratefully acknowledge support for this research from NSF Awards IIP1034710, IIP1822130 and DTRA contract # HDTRA 1-16-1-0028. This research was carried out in the NSF Industry/University Cooperative Research Center for Membrane Science, Engineering and Technology that has been supported via two NSF Awards IIP1034710 and IIP-1822130. The authors thank Amedeo Napolitano and Matt Browe for conducting the chlorine micro-breakthrough tests as well as CEES permeation tests.

Appendix A. Supplementary material

Supplementary data to this article can be found online at https://doi.org/10.1016/j.seppur.2020.117406.

References

[1] R. Nagarajan, W. Zukas, T.A. Hatton, S. Lee (Eds.), Nanoscience and nanotechnology for chemical and biological defense. In: ACS Symposium Series, vol. 1016. American Chemical Society, 2009.
[2] P. Kikilo, V. Fedorenko, A.L. Ternay, Chemical warfare agents: chemistry, pharmacology, toxicology, and therapeutics, CRC Press, 2007, pp. 21–50.
[3] E. Napadensky, Y.A. Elabd, Breathability and selectivity of selected materials for protective clothing. No. ARL-TR-3235. Army Research Lab Aberdeen Proving Ground, MD Weapons Mater. Res. Directorate (2004).
[4] M.A. Wartell, M.A. Wartell, M.T. Kleinman, B.M. Huey, L.M. Duffy, Strategies to Protect the Health of Deployed U.S. Forces: Force Protection and Decontamination, National Academy Press, Washington, D.C., 1999.
[5] G.R. Lomax, Breathable polyurethane membranes for textile and related industries, J. Mater. Chem. 17 (27) (2007) 2775–2784.
[6] M. Rother, J. Barmettler, A. Reichmuth, J.V. Araujo, C. Rytka, O. Glaied, U. Pieles, N. Bruns, Self-Sealing and Puncture Resistant Breathable Membranes for Water-Evaporation Applications, Adv. Mater. 27 (42) (2015) 6620–6624.
[7] Approval of Respiratory Protective Devices. Code of Federal Regulations, Part 84, Title 42, 1995.
[8] N. Bui, E.R. Meshot, S. Kim, J. Peña, P.W. Gibson, K.J. Wu, F. Fornasiero, Ultrabreathable and protective membranes with sub-5 nm carbon nanotube pores, Adv. Mater. 28 (2016) 5871–5877.
[9] F. Fornasiero, Water vapor transport in carbon nanotube membranes and application in breathable and protective fabrics, Curr. Opin. Chem. Eng. 16 (2017) 1–8.
[10] G.W. Peterson, J.B. DeCoste, F. Fatollahi-Fard, D.K. Britt, Engineering UiO-66-NH_2 for toxic gas removal, Ind. Eng. Chem. Res. 53 (2) (2014) 701–707.
[11] H. Jasuja, G.W. Peterson, J.B. Decoste, M.A. Browe, K.S. Walton, Evaluation of MOFs for air purification and air quality control applications: Ammonia removal from air, Chem. Eng. Sci. 124 (2015) 118–124.
[12] A.J. Rieth, M. Dincă, Controlled Gas Uptake in Metal-Organic Frameworks with Record Ammonia Sorption, J. Am. Chem. Soc. 140 (9) (2018) 3461–3466.
[13] A.J. Rieth, M. Dincă, Programming framework materials for ammonia capture, ACS Cent Sci. 4 (6) (2018) 666–667.
[14] S. Sorribas, P. Gorgojo, C. Téllez, J. Coronas, A.G. Livingston, High flux thin film nanocomposite membranes based on metal-organic frameworks for organic solvent nanofiltration, J. Am. Chem. Soc. 135 (40) (2013) 15201–15208.
[15] M. Kadhom, W. Hu, B. Deng, Thin film nanocomposite membrane filled with metal-organic frameworks UiO-66 and MIL-125 nanoparticles for water desalination, Membranes 7 (2) (2017) 31.
[16] K. Eum, C. Ma, A. Rownaghi, C.W. Jones, S. Nair, ZIF-8 Membranes via interfacial microfluidic processing in polymeric hollow fibers: Efficient propylene separation at elevated pressures, ACS Appl. Mater. Interfaces 8 (38) (2016) 25337–25342.
[17] Z. Zhao, X. Ma, A. Kasik, Z. Li, Y.S. Lin, Gas separation properties of metal organic framework (MOF-5) membranes, Ind. Eng. Chem. Res. 52 (3) (2012) 1102–1108.
[18] Y.S. Lin, Metal organic framework membranes for separation applications, Curr. Opin. Chem. Eng. 8 (2015) 21–28.
[19] J.Y. Lin, Molecular sieves for gas separation, Science 353 (6295) (2016) 121–122.
[20] A.S. Kovvali, H. Chen, K.K. Sirkar, Dendrimer membranes: A CO_2-selective molecular gate, J. Am. Chem. Soc. 122 (2000) 7594–7595.
[21] J.H. Cavka, J. Søren, O. Unni, G. Nathalie, L. Carlo, B. Silvia, P.L. Karl, A new zirconium inorganic building brick forming metal organic frameworks with exceptional stability, J. Am. Chem. Soc. 130 (42) (2008) 13850–13851.
[22] M. Kandiah, H.N. Merete, U. Sandro, J. Søren, O. Unni, T. Mats, L. Cherif, A.Q. Elsje, B. Francesca, P.L. Karl, Synthesis and stability of tagged UiO-66 Zr-MOFs, Chem. of Mater. 22 (24) (2010) 6632–6640.
[23] A.M. Ploskonka, S.E. Marzen, J.B. DeCoste, Facile Synthesis and Direct Activation of Zirconium Based Metal-Organic Frameworks from Acetone, Ind. Eng. Chem. Res. 56 (6) (2017) 1478–1484.
[24] G.W. Peterson, M.A. Browe, E.M. Durke, T.H. Epps III, Flexible SIS/HKUST-1 Mixed Matrix Composites as Protective Barriers against Chemical Warfare Agent Simulants, ACS Appl. Mater. Interfaces 10 (2018) 43080–43087.
[25] C. Peng, Z. Iqbal, K.K. Sirkar, G.W. Peterson, Graphene oxide-based membrane as protective barrier against toxic vapors and gases, ACS Appl. Mater. Interfaces 12 (9) (2020) 11094–11103.
[26] P.W. Gibson, C.E. Kendrick, Rivin D.; Sicuranza L.; Charmchi M. An Automated Dynamic Water Vapor Permeation Test Method. No. NATICK/TR-95/032, J. Coated Fabrics 24 (1995) 322–345.
[27] G.W. Peterson, A.X. Lu, T.H. Epps III, Tuning the Morphology and Activity of Electrospun Polystyrene/UiO-66-NH_2 Metal−Organic Framework Composites to Enhance Chemical Warfare Agent Removal, ACS Appl. Mater. Interfaces 9 (2017) 32248–32254.
[28] NIST Chemistry Web book, SRD69: https://webbook.nist.gov/cgi/cbook.cgi?ID=B6002270&Mask=80.
[29] H.R. Abida, J. Shang, H.-M. Anga, S. Wang, Amino-functionalized Zr-MOF nanoparticles for adsorption of CO_2 and CH_4, Int. J. Smart Nano Mater. 4 (1) (2013) 72–82.
[30] V. Dubey, Maiti S.N.; Rao N.B.; Gupta A.K.; Study of permeation of bis (2-chloroethyl) sulfide through elastomer membranes, Polymer—Plastics Technol. Eng. 36 (3) (1997) 445–460.